ACS APPLIED ENERGY MATERIALS

www.acsaem.org Letter

Indium Gallium Oxide Emitters for High-Efficiency CdTe-Based Solar Cells

Manoj K. Jamarkattel, Adam B. Phillips,* Indra Subedi, Abasi Abudulimu, Ebin Bastola, Deng-Bing Li, Xavier Mathew, Yanfa Yan, Randy J. Ellingson, Nikolas J. Podraza, and Michael J. Heben

Cite This: https://doi.org/10.1021/acsaem.2c00153 Read Online

ACCESS | Metrics & More | Article Recommendations | Supporting Information

ABSTRACT: There are limited choices for front-surface, electron-selective contacts (emitters) for CdTe solar cells, thus hindering scientific and technical development. Here we investigate the photovoltaic performance of devices fabricated with $(In_xGa_{1-x})_2O_3$ (IGO) emitters with varying In-to-Ga ratios prepared by cosputtering. In agreement with predictions, an IGO emitter with a 4.03 eV bandgap (x = 0.36) allowed fabrication of devices with efficiencies of 16%. Increasing the performance to higher values will be enabled by increasing the transmission through the IGO-coated substrate and decreasing the bulk and back interface recombination. These findings demonstrate IGO materials as effective emitters in high-efficiency CdTe-based solar cells.

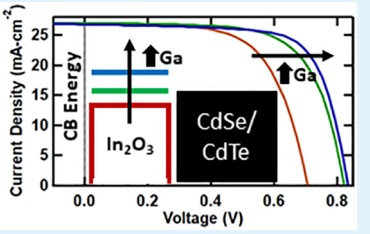

KEYWORDS: *CdTe, photovoltaics, emitter, indium gallium oxide, front interface, band alignment*

CdTe has emerged as the leading thin-film photovoltaics (PV) technology because of its unique combination of long-term stability, low-cost manufacturing, and high efficiency. From 2011 to 2016, the record cell efficiency increased dramatically from 16.3 to 22.1% with the implementation of several advances, resulting in follow-on increases in large module performance up to 19.0%.[1] In particular, the introduction of Se into the front of the device extended the wavelength in the quantum efficiency while also increasing the carrier lifetime.[2,3] The recent experimental advances have transformed the outlook for the device evolution, with many investigators now working toward efficiencies beyond 25%.[4−6]

Device research is now progressing on several fronts, including efforts to increase absorber carrier concentrations[7,8] and lifetimes[9] and the fabrication of electron- and hole-selective contacts with low interfacial carrier recombination rates. The rear contact, which extracts holes, has received substantial attention over the years because it is readily accessible.[10] The superstrate configuration in which the device is manufactured and the p-type conductivity of the vapor-deposited CdTe dictates that the rear hole contact is fabricated last.

Improvements in the front emitter's performance have clearly been made in the record devices, but details of the materials and processes are not available in the open literature. Synthetic control tuned to final low-recombination performance is very difficult to achieve because of the technical challenges associated with fabrication. Growth of a high-efficiency CdTe-based absorber layer is typically done at temperatures near 600 °C, and the postdeposition $CdCl_2$ activation treatment is typically done near 400 °C. Consequently, any buffer layers interposed between the transparent conducting oxide-coated glass substrate and the semiconductor layer must be thermally stable and relatively unreactive. The structure of the emitter contact used in the record 22.1% device is not openly known, but it is likely based on a stack comprising transparent conducting oxide (TCO, e.g., F-doped SnO_2) overlaid with an undoped buffer layer, as has historically been the case.

Recent modeling has shown that band and Fermi level alignment between the front interface emitter and the absorber is necessary for low front interfacial recombination currents and high efficiency.[11,12] When the conduction band and Fermi level of the emitter are relatively high in energy as compared to those of the absorber, the conduction band offset (CBO) is assigned to be positive and the band bending that drives the majority carrier holes away from the front interface is increased in the absorber. To date, only one buffer material system, consisting of combinations of MgO and ZnO (i.e., $Mg_xZn_{1-x}O$), has been communicated in the literature with the ability to tune the CBO and reduce front interface recombination to achieve efficiencies as high as 19.5%.[13]

A recent modeling paper by Dive et al. suggested that the materials in the In_2O_3−Ga_2O_3 system could possibly be a second potential candidate materials system for CdTe emitter fabrication.[14] Although the component oxides, In_2O_3 and Ga_2O_3, have bandgaps between 2.9 and 3.6 eV[15−18] and 4.5−

Received: January 13, 2022
Accepted: April 19, 2022

4.9 eV[19−23] and would form negative and large positive CBOs with CdTe, respectively, an alloy of composition $(In_xGa_{1-x})_2O_3$ (IGO) should allow the CBO and bandgap to be continuously varied. In fact, recent numerical modeling indicates that a high efficiency emitter for CdTe should be achievable with the $InGaO_3$ composition with a bandgap of ~4 eV, but no experimental work has verified the modeled results.

Here, we present an experimental examination of IGO materials for use as emitters in CdTe-based solar cells. The composition and bandgap of the film was varied by cosputtering the IGO films from In_2O_3 and Ga_2O_3 targets. We show that the open circuit voltage (V_{OC}) is low at high indium fraction and increases and saturates at 0.833 V when x reaches 0.45. The fill factor, on the other hand, peaks at x = 0.36. These results are consistent with a conduction band edge that increases in energy with decreasing indium fraction. Device efficiencies greater than 16% were achieved when the indium fraction was 0.36, which corresponds to a bandgap of 4.02 eV. By analyzing the current density−voltage (J−V) and external quantum efficiency (EQE) curves, we determine that the device performance is not limited by the front interface.

IGO films with various compositions were prepared by cosputtering from In_2O_3 and Ga_2O_3 targets in an Ar/O_2 environment onto substrates held at 250 °C. The composition of the films was varied by adjusting the power on each target (see the Supporting Information for details). All films were transparent to the eye as-deposited.

A combination of spectroscopic ellipsometry and normal incidence transmission measurements was used to determine the absorption coefficient from the imaginary part of the refractive index of the films grown on soda lime glass. Tauc plots were constructed from the absorption coefficient data to determine the direct bandgaps. The composition of the film was determined using energy-dispersive X-ray spectroscopy.

Figure 1a shows the measured bandgap (E_g) data plotted as a function indium fraction (x) in $(In_xGa_{1-x})_2O_3$. The values we measured for pure In_2O_3 (3.30 eV) and Ga_2O_3 (4.77 eV) films are in the middle of the ranges that have been reported for In_2O_3 (2.9−3.6 eV[15,16]) and Ga_2O_3 (4.5−4.9 eV[19−23]). The dotted curve in Figure 1a shows that the data are nicely fit between the pure compound limits by an expression that considers band bowing during alloying (eq 1).

$$E_g = E_g^{Ga_2O_3}(1 - x) + E_g^{In_2O_3}x - b(1 - x)x \quad (1)$$

Here, the best fit was found when b, the bowing coefficient, was 1.18 eV. Figure 1a also shows data from other investigations. In comparison to other experimental efforts, our data have the same general trend of variation in the indium fraction with somewhat lower bandgaps, particularly at the higher indium contents. A key difference may be that our samples were prepared by cosputtering at a relatively low substrate temperature of 250 °C, whereas most other experimental work to date has employed pulsed laser deposition (PLD) on substrates heated to 650 °C.[21−23] Although the PLD approach yields crystalline films that exhibit X-ray diffraction spectra, our cosputtered samples are amorphous in the as-deposited state.

Figure 1b shows the resistivity of 150 nm IGO films on soda lime glass as a function of In fraction. For the as-deposited films, the resistivity of only three films could be measured, though the resistance of the film with x = 0.45 was near the upper limit of the four point probe system. After the films went

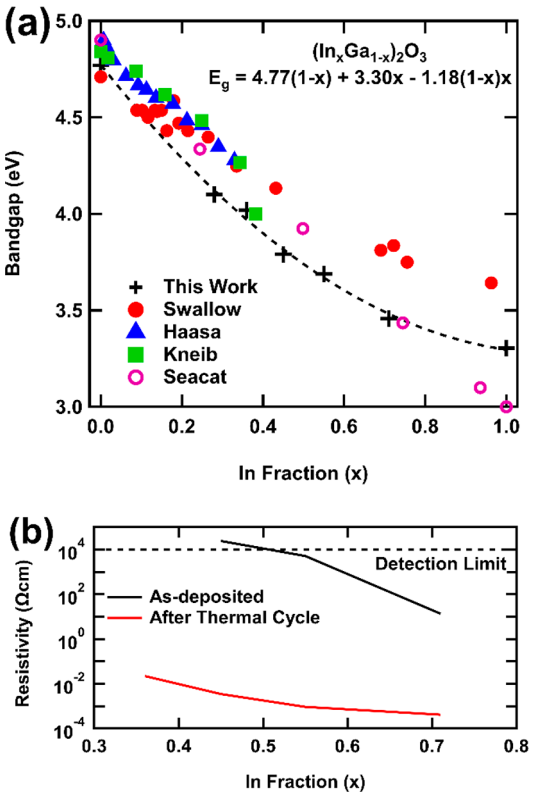

Figure 1. (a) Bandgap of $(In_xGa_{1-x})_2O_3$ as a function of x. The + symbols show the values measured in this work in comparison to other reports (refs 21−24). (b) Resistivity of 150 nm IGO films as a function of x after deposition and completing the deposition thermal cycle completed without source material.

through the high temperature thermal cycle used during vacuum deposition (see the Supporting Information), the resistivity of all films decreased by orders of magnitude. Although these values may increase after $CdCl_2$ activation, the resistivity after undergoing the deposition thermal cycle suggests that the doping in the IGO films can be sufficiently high for the device performance to follow that of the models.[11,14]

For devices, 75 nm thick IGO films of selected compositions (x = 0.28, 0.36, 0.45, 0.55, and 0.71) were deposited onto clean F-doped SnO_2 (FTO) coated glass. A 150 nm layer of CdSe was sputtered onto the IGO at room temperature followed by deposition of 3.5 μm CdTe using a closed space sublimation. The devices were $CdCl_2$ activated, Cu doped using a $CuCl_2$ solution, and finished with Au (see the Supporting Information for details.)

Figure 2 shows the PV response parameters for the devices as a function of the IGO bandgap, and Figures 3b and 4 show the J−V and EQE curves of the best devices for each emitter composition, respectively. From Figure 2, we see that for the lowest bandgap IGO emitter investigated here (E_g = 3.46 eV, x = 0.71), the average V_{OC} is very low at 0.617 V. When the bandgap is increased to 3.69 and 3.80 eV, the average V_{OC} increases to 0.701 and 0.826 V, respectively. A further increase in bandgap leads to only a small increase in V_{OC}, which appears to saturate at 0.833 V. The J−V results suggest the band alignment at the front interface improves with increasing IGO bandgap. Although the fraction of bandgap increase accommodated by an increase in the conduction band has been estimated to be between 25 and 66% using density functional

https://doi.org/10.1021/acsaem.2c00153
ACS Appl. Energy Mater. XXXX, XXX, XXX−XXX

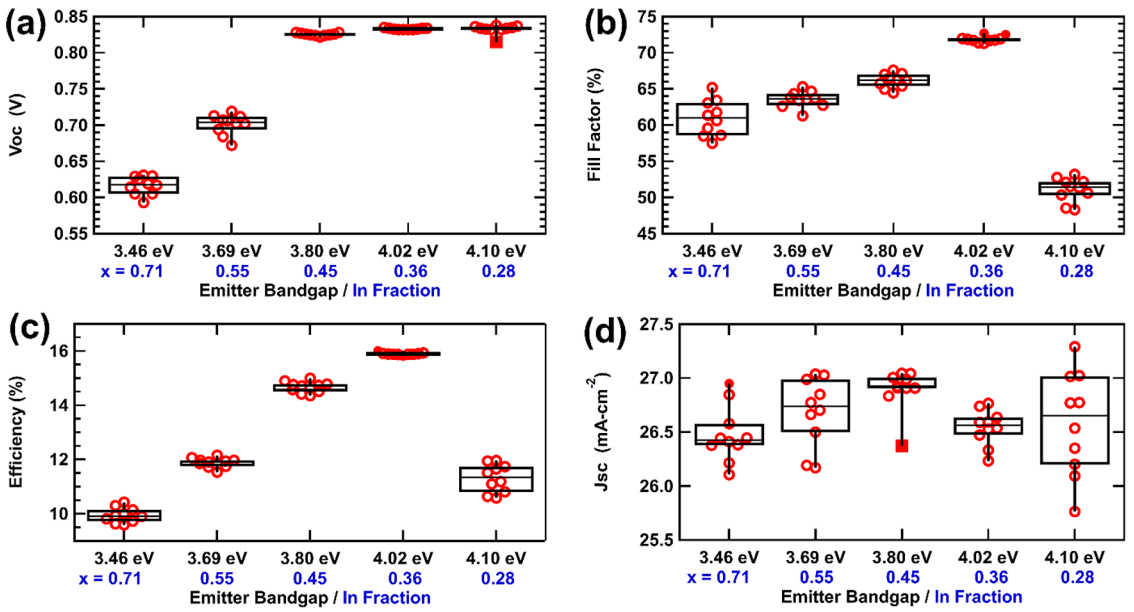

Figure 2. (a) Open circuit voltage (V_{OC}), (b) fill factor, (c) efficiency, and (d) short circuit current density (J_{SC}) of Tec 10/75 nm $(In_xGa_{1-x})_2O_3$ (IGO)/3.6 μm $CdSe_yTe_{1-y}$/$CuCl_2$/50 nm Au devices for varying IGO bandgaps/x values.

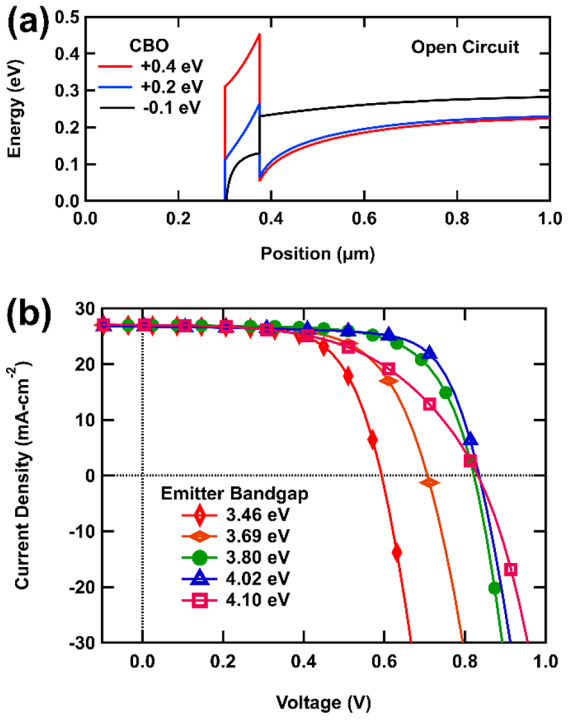

Figure 3. (a) Conduction band portion of band diagram near the front interface of devices with varying conduction band offsets (CBOs) shown at open circuit. (b) The current density−voltage (J−V) curves of the best devices with each IGO composition.

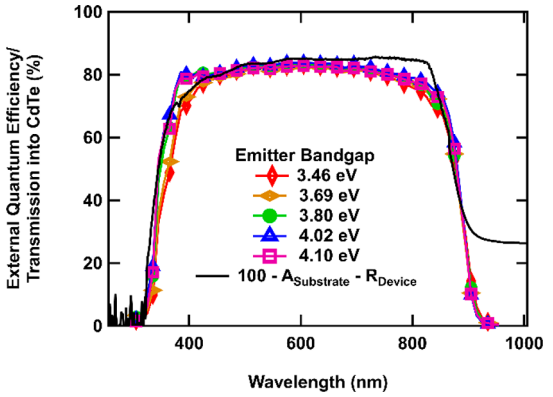

Figure 4. External quantum efficiency (EQE) curves of the best devices with each IGO composition. Also shown is the transmission of light into the absorber layer for an emitter layer bandgap of 3.80 eV (black, no symbols).

theory,[14,23,24] the change in V_{OC} of ∼0.210 V observed with a bandgap increase of 0.34 eV is consistent with the conduction band change accounting for half of the overall bandgap change. The saturation in V_{OC} suggests that the conduction band of the IGO with a bandgap of 3.80 is approximately equal to the conduction band of the CdTe, at ∼4.4 eV down from the vacuum level.

Although the V_{OC} saturates when the emitter bandgap is 3.80 eV, the fill factor (FF) continues to increase to 71.9% when the IGO bandgap is 4.02 eV. The increase in FF means that the bias-dependent recombination decreases. The increase in bandgap due to a higher Ga fraction moves the conduction band and Fermi level closer to the vacuum level and farther from the Fermi level of the p-type CdTe absorber. When the p−n junction is formed, this leads to an increase in band bending in the absorber at the front interface. The increased FF observed for lower IGO bandgaps is consistent with an increase in band bending in the absorber. Once the Fermi level of the emitter is higher in energy than the conduction band of the absorber, though, the overall band bending in the absorber becomes constant; however, as the band diagrams in Figure 3a show, the local band bending near the front interface continues to increase with the conduction band offset. As a result, increasing the IGO bandgap from 3.80 to 4.02 eV continues to improve FF. At some emitter bandgap, the large conduction band offset impedes electron flow from the absorber into the emitter, thereby trapping holes in the absorber where they recombine. This may be occurring when the bandgap increases to 4.10 eV.

https://doi.org/10.1021/acsaem.2c00153
ACS Appl. Energy Mater. XXXX, XXX, XXX−XXX

Looking at the $J-V$ curve shown in Figure 3b, we see the slight change in slope that occurs just above V_{OC} that may signal the emergence of a so-called S-kink when the bandgap is 4.10 eV, which is indicative of a barrier that prevents the extraction of electrons.[11] In the $J-V$ curve, the bias at which the collected current begins to decrease provides information on the height of the barrier. At all biases, the following condition must be met

$$J = J_{ph} - J_{Bulk} - J_{Front} - J_{Back} \quad (2)$$

where J_{ph} is the photogenerated current density and J_{Bulk}, J_{Front}, and J_{Back} are the recombination current densities due to recombination in the bulk, at the front interface, and at the back interface, respectively. Because J_{ph} is constant for each device, the loss in fill factor indicates that one of the recombination mechanisms turns on at an earlier bias, and because the back interface is the same in all device, the loss in J must be due to bulk or front interface recombination. From the band diagram point of view, too large of a conduction band offset between the emitter and absorber prevent electrons from leaving the absorber, thereby leading to recombination in the bulk at early biases.[11,14] Consequently, the maximum power point should shift to lower bias as the bandgap of the emitter increases, as observed here.

This sudden drop in FF for a bandgap increase of 0.08 eV suggests that an emitter bandgap of 4.02 eV is very close to the "optimum" conduction band offset based on the modeling results.[11] However, the performance of devices that use an MZO emitter does not always follow this model. Many groups have observed a so-called S-kink and significant drop in FF for MZO bandgaps/compositions that should only create a small barrier on the order of +0.1−0.2 eV. For some devices, the S-kink appears to be related to the carrier concentration and Fermi level position in the MZO even when only a small positive CBO exists[25,26] when the doping level in MZO is controlled by oxygen vacancy concentration. Others have noted that the S-kink in the MZO devices can also be due to metastability in the MZO due to the formation of MgO during processing.[27,28] Thus, both mechanisms depend on device processing, especially when $CdCl_2$ activation is done in air. We note that the devices reported here were $CdCl_2$ activated in air and illuminated with an LED solar simulator with a 400 nm low wavelength cutoff but do not show any S-kink-like behavior until the bandgap of the emitter is 4.10 eV. This is in direct contrast to a device fabricated using the same deposition steps with an "ideal" bandgap $Mg_{0.23}Zn_{0.77}O$ emitter[29] and processed under the same conditions, which shows a strong S-kink (see the Supporting Information). However, for IGO, the structure change from hexagonal to monoclinic is expected to occur for $x \approx 0.3$,[23] and the FF drop occurs when x is between 0.36 and 0.28. Although X-ray diffraction measurements of the IGO films after undergoing the deposition thermal cycle did not show any peaks, the film may consist of crystallites with insufficient long-range order to yield a diffraction pattern. In an attempt to determine the location of the additional recombination, we performed steady state photoluminescence (PL) measurements of the completed devices (see the Supporting Information). Interestingly, these results more closely follow the FF than the V_{OC} trends. This drop in PL response as the emitter bandgap increases from 4.02 to 4.10 eV suggests that more photogenerated carriers recombine near the front interface with the wider bandgap emitter. Consequently, although theory predicts that this bandgap would result in a CBO greater than +0.3 eV, and thus present a large barrier to electron flow at the front interface,[14,23,24] we cannot rule out the possibility that the fill factor loss we observe could be due to a moderate barrier coupled with unoptimized doping in the emitter or a structure change of the oxide, as is often observed with MZO.

Although the overall trends in the V_{OC} and FF are promising, other aspects of the devices could be improved. Most striking is the low J_{SC} at ∼26.5 mA cm^{-2}. We note that similar devices prepared on a FTO substrate with higher transparency (Tec 12D) exhibited J_{SC} values of 27.9 mA cm^{-2}.[9] Turning to the EQE data shown in Figure 4 to determine where J_{SC} is lost, we see that the long wavelength edge goes to ∼900 nm, indicating that the near-front-surface bandgap value of 1.38 eV has been achieved, as expected for optimal $CdSe_xTe_{1-x}$ alloying. J_{SC} values of ∼29.0 mA cm^{-2} have been achieved in similar devices without the use of an antireflective coating.[30] The EQE data shows a slight downward slope in the long wavelength range. Although this can be improved, it does not account for the full ∼2.5 mA cm^{-2} loss in J_{SC}, nor does the slight deviation for two narrower bandgap IGO emitters at short wavelength. Most of the J_{SC} loss appears to be due to reduce EQE for all wavelengths, with a peak ∼82%. However, this peak value is very close to the value of the light incident on the absorber (Figure 4, black line), suggesting that the internal quantum efficiency for wavelengths up to ∼700 nm is very high for these devices. In fact, for the amount of light incident upon the absorber the integrated J_{SC} is 26.9 mA cm^{-2}, and the difference in the long wavelength range between the incident light and measured EQE yields a J_{SC} loss of 0.4 mA cm^{-2}, which agrees with the measured value. Clearly, improving J_{SC} will require reducing the absorbance of the FTO/IGO superstrate and the reflection off the device stack by changing the superstrate or modifying the IGO deposition parameters and/or thickness.

The V_{OC} and FF are also lower than expected for a good front interface. These values, though, are in line with what has been measured for devices fabricated using the same methods on Tec 12D superstrates.[9] There, the V_{OC} and FF for the device finished with just a $CuCl_2$/Au back contact were 0.839 V and 70.6%, respectively. The V_{OC} is 6 mV higher in that case, but this may be due to the higher J_{SC} obtained for those devices (27.9 mA cm^{-2}) or sample-to-sample variation. Incorporating a Cu_xAlO_y buffer layer led to a significant increase in both V_{OC} and FF, so the low V_{OC} and FF observed in those devices finished with $CuCl_2$/Au were due to a combination of the doping and recombination at the back interface. Because the only difference in device stacks used in our previous work and here is the replacement of the high resistance transport (HRT) layer with an IGO layer, we expect the absorber and back interfaces to be identical and, therefore, conclude the V_{OC} of the devices presented in this manuscript are also limited by recombination in the bulk or at the back interface.

In summary, we present the first experimental evidence that IGO materials can serve as an emitter layer in high efficiency CdTe solar cells. The V_{OC} increases with IGO bandgap until a saturation value of 0.833 V is reached. The FF increases with bandgap and reaches a maximum value of 71.9 at 4.02 eV. These results are consistent with improved band alignment at the front interface and indicate an IGO bandgap of ∼4 eV, which occurs when the In fraction x is ∼0.36, is near optimal for devices. Although the internal quantum efficiency of the

https://doi.org/10.1021/acsaem.2c00153
ACS Appl. Energy Mater. XXXX, XXX, XXX−XXX

devices is high, the short circuit current is limited by absorption in the FTO/IGO superstrate. Comparison with other devices suggest that the values reported here are not limited by front surface recombination, although recombination at the front does appear to affect the FF for the widest bandgap emitter. Although several routes exist for increasing the device efficiency further, the current configuration exhibits an efficiency of 16.1%.

■ ASSOCIATED CONTENT

Supporting Information

The Supporting Information is available free of charge at https://pubs.acs.org/doi/10.1021/acsaem.2c00153.

Additional experimental details, methods, and materials; $J-V$ response of the device with an MZO emitter; steady-state photoluminescence data of the devices (PDF)

■ AUTHOR INFORMATION

Corresponding Author

Adam B. Phillips − *Wright Center for Photovoltaic Innovation and Commercialization, Department of Physics and Astronomy, University of Toledo, Toledo, Ohio 43606, United States;* orcid.org/0000-0002-2675-5052; Email: adam.phillips@utoledo.edu

Authors

Manoj K. Jamarkattel − *Wright Center for Photovoltaic Innovation and Commercialization, Department of Physics and Astronomy, University of Toledo, Toledo, Ohio 43606, United States;* orcid.org/0000-0003-2767-5705

Indra Subedi − *Wright Center for Photovoltaic Innovation and Commercialization, Department of Physics and Astronomy, University of Toledo, Toledo, Ohio 43606, United States;* orcid.org/0000-0003-2300-6010

Abasi Abudulimu − *Wright Center for Photovoltaic Innovation and Commercialization, Department of Physics and Astronomy, University of Toledo, Toledo, Ohio 43606, United States;* orcid.org/0000-0002-1794-0993

Ebin Bastola − *Wright Center for Photovoltaic Innovation and Commercialization, Department of Physics and Astronomy, University of Toledo, Toledo, Ohio 43606, United States;* orcid.org/0000-0002-4194-3385

Deng-Bing Li − *Wright Center for Photovoltaic Innovation and Commercialization, Department of Physics and Astronomy, University of Toledo, Toledo, Ohio 43606, United States;* orcid.org/0000-0003-4555-4894

Xavier Mathew − *Wright Center for Photovoltaic Innovation and Commercialization, Department of Physics and Astronomy, University of Toledo, Toledo, Ohio 43606, United States; Instituto de Engergías Renovables, Universidad Nacional Autónoma de México, Temixco, Morelaos 62580, México;* orcid.org/0000-0002-3017-5552

Yanfa Yan − *Wright Center for Photovoltaic Innovation and Commercialization, Department of Physics and Astronomy, University of Toledo, Toledo, Ohio 43606, United States;* orcid.org/0000-0003-3977-5789

Randy J. Ellingson − *Wright Center for Photovoltaic Innovation and Commercialization, Department of Physics and Astronomy, University of Toledo, Toledo, Ohio 43606, United States;* orcid.org/0000-0001-9520-6586

Nikolas J. Podraza − *Wright Center for Photovoltaic Innovation and Commercialization, Department of Physics and Astronomy, University of Toledo, Toledo, Ohio 43606, United States*

Michael J. Heben − *Wright Center for Photovoltaic Innovation and Commercialization, Department of Physics and Astronomy, University of Toledo, Toledo, Ohio 43606, United States;* orcid.org/0000-0002-3788-3471

Complete contact information is available at: https://pubs.acs.org/10.1021/acsaem.2c00153

Notes

The authors declare no competing financial interest.

■ ACKNOWLEDGMENTS

This material is based on research sponsored by the Air Force Research Laboratory under agreements FA9453-19-C-1002 and FA9453-21-C-0056. Public Affairs release approval #AFRL-2022-1551. The views and conclusions contained herein are those of the authors and should not be interpreted as necessarily representing the official policies or endorsements, either expressed or implied, of Air Force Research Laboratory or the U.S. Government.

■ REFERENCES

(1) https://www.nrel.gov/pv/cell-efficiency.html.(accessed 2022-01-10).

(2) Paudel, N. R.; Yan, Y. F. Enhancing the Photo-Currents of CdTe Thin-Film Solar Cells in Both Short and Long Wavelength Regions. *Appl. Phys. Lett.* **2014**, *105* (18), 183510.

(3) Kephart, J. M.; Kindvall, A.; Williams, D.; Kuciauskas, D.; Dippo, P.; Munshi, A.; Sampath, W. S. Sputter-Deposited Oxides for Interface Passivation of CdTe Photovoltaics. *IEEE J. Photovolt.* **2018**, *8* (2), 587−593.

(4) Kanevce, A.; Reese, M. O.; Barnes, T. M.; Jensen, S. A.; Metzger, W. K. The Roles of Carrier Concentration and Interface, Bulk, and Grain-Boundary Recombination for 25% Efficient CdTe Solar Cells. *J. Appl. Phys.* **2017**, *121* (21), 214506.

(5) Ablekim, T.; Colegrove, E.; Metzger, W. K. Interface Engineering for 25% CdTe Solar Cells. *ACS Applied Energy Materials* **2018**, *1* (10), 5135−5139.

(6) Liyanage, G. K.; Phillips, A. B.; Alfadhili, F. K.; Ellingson, R. J.; Heben, M. J. The Role of Back Buffer Layers and Absorber Properties for > 25% Efficient CdTe Solar Cells. *ACS Applied Energy Materials* **2019**, *2* (8), 5419−5426.

(7) McCandless, B. E.; Buchanan, W. A.; Thompson, C. P.; Sriramagiri, G.; Lovelett, R. J.; Duenow, J.; Albin, D.; Jensen, S.; Colegrove, E.; Moseley, J.; et al. Overcoming Carrier Concentration Limits in Polycrystalline CdTe Thin Films with In Situ Doping. *Sci. Rep* **2018**, *8* (1), 14519.

(8) Metzger, W. K.; Grover, S.; Lu, D.; Colegrove, E.; Moseley, J.; Perkins, C. L.; Li, X.; Mallick, R.; Zhang, W.; Malik, R.; Kephart, J.; Jiang, C. S.; Kuciauskas, D.; Albin, D. S.; Al-Jassim, M. M.; Xiong, G.; Gloeckler, M. Exceeding 20% Efficiency with in situ Group V Doping in Polycrystalline CdTe Solar Cells. *Nature Energy* **2019**, *4* (10), 837−845.

(9) Jamarkattel, M. K.; Phillips, A. B.; Khanal Subedi, K.; Bastola, E.; Gibbs, J. M.; Friedl, J. D; Rijal, S.; Pokhrel, D.; Awni, R. A.; Li, D.-B.; et al. Improving CdSeTe Devices With a Back Buffer Layer of Cu_xAlO_y. *IEEE Journal of Photovoltaics* **2022**, *12*, 1−6.

(10) Hall, R. S.; Lamb, D.; Irvine, S. J. C. Back Contacts Materials Used in Thin Film CdTe Solar Cells—A Review. *Energy Science & Engineering* **2021**, *9* (5), 606−632.

(11) Song, T.; Kanevce, A.; Sites, J. R. Emitter/Absorber Interface of CdTe Solar Cells. *J. Appl. Phys.* **2016**, *119* (23), 233104.

(12) Pandey, R.; Shimpi, T.; Munshi, A.; Sites, J. R. Impact of Carrier Concentration and Carrier Lifetime on MgZnO/CdSeTe/CdTe Solar Cells. *IEEE Journal of Photovoltaics* **2020**, *10* (6), 1918−1925.
(13) Yeung, G.; Reich, C.; Onno, A.; Bothwell, A.; Danielson, A.; Holman, Z.; Sampath, W. S.; Wolden, C. A. Robust Passivation of CdSeTe Based Solar Cells Using Reactively Sputtered Magnesium Zinc Oxide. *Sol. Energy Mater. Sol. Cells* **2021**, *233*, 111388.
(14) Dive, A.; Varley, J.; Banerjee, S. In2O3-Ga2O3 Alloys as Potential Buffer Layers in CdTe Thin-Film Solar Cells. *Physical Review Applied* **2021**, *15* (3), 034028.
(15) Zhang, F.; Saito, K.; Tanaka, T.; Nishio, M.; Guo, Q. Wide Bandgap Engineering of $(GaIn)_2O_3$ Films. *Solid State Commun.* **2014**, *186*, 28−31.
(16) Müller, H. K. Electrical and Optical Properties of Sputtered In_2O_3 films. I. Electrical Properties and Intrinsic Absorption. *Physica status solidi (b)* **1968**, *27* (2), 723−731.
(17) Irmscher, K.; Naumann, M.; Pietsch, M.; Galazka, Z.; Uecker, R.; Schulz, T.; Schewski, R.; Albrecht, M.; Fornari, R. On the Nature and Temperature Dependence of the Fundamental Band Gap of In_2O_3. *Physica status solidi (a)* **2014**, *211* (1), 54−58.
(18) Ellmer, K. Past Achievements and Future Challenges in the Development of Optically Transparent Electrodes. *Nat. Photonics* **2012**, *6* (12), 809−817.
(19) Rebien, M.; Henrion, W.; Hong, M.; Mannaerts, J. P.; Fleischer, M. Optical Properties of Gallium Oxide Thin Films. *Appl. Phys. Lett.* **2002**, *81* (2), 250−252.
(20) Mobtakeri, S.; Akaltun, Y.; Özer, A.; Kılıç, M.; Tüzemen, E. Ş.; Gür, E. Gallium Oxide Films Deposition by RF Magnetron Sputtering; a Detailed Analysis on the Effects of Deposition Pressure and Sputtering Power and Annealing. *Ceram. Int.* **2021**, *47* (2), 1721−1727.
(21) Hassa, A.; von Wenckstern, H.; Splith, D.; Sturm, C.; Kneiß, M.; Prozheeva, V.; Grundmann, M. Structural, Optical, and Electrical Properties of Orthorhombic κ-$(In_xGa_{1-x})_2O_3$ Thin Films. *APL Materials* **2019**, *7* (2), 022525.
(22) Kneiß, M.; Hassa, A.; Splith, D.; Sturm, C.; von Wenckstern, H.; Lorenz, M.; Grundmann, M. Epitaxial Stabilization of Single Phase κ-$(In_xGa_{1-x})_2O_3$ Thin Films up to x = 0.28 on c-Sapphire and κ-Ga_2O_3 (001) Templates by Tin-Assisted VCCS-PLD. *APL Materials* **2019**, *7* (10), 101102.
(23) Swallow, J. E. N.; Palgrave, R. G.; Murgatroyd, P. A. E.; Regoutz, A.; Lorenz, M.; Hassa, A.; Grundmann, M.; von Wenckstern, H.; Varley, J. B.; Veal, T. D. Indium Gallium Oxide Alloys: Electronic Structure, Optical Gap, Surface Space Charge, and Chemical Trends within Common-Cation Semiconductors. *ACS Appl. Mater. Interfaces* **2021**, *13* (2), 2807−2819.
(24) Seacat, S.; Lyons, J. L.; Peelaers, H. Properties of Orthorhombic Ga_2O_3 Alloyed with In_2O_3 and Al_2O_3. *Appl. Phys. Lett.* **2021**, *119* (4), 042104.
(25) Pandey, R.; Shah, A.; Munshi, A.; Shimpi, T.; Jundt, P.; Guo, J.; Klie, R. F.; Sampath, W.; Sites, J. R. Mitigation of J−V Distortion in CdTe Solar Cells by Ga-doping of MgZnO Emitter. *Sol. Energy Mater. Sol. Cells* **2021**, *232*, 111324.
(26) Li, D.-B.; Song, Z.; Awni, R. A.; Bista, S. S.; Shrestha, N.; Grice, C. R.; Chen, L.; Liyanage, G. K.; Razooqi, M. A.; Phillips, A. B.; Heben, M. J.; Ellingson, R. J.; Yan, Y. Eliminating S-Kink To Maximize the Performance of MgZnO/CdTe Solar Cells. *ACS Applied Energy Materials* **2019**, *2* (4), 2896−2903.
(27) Bittau, F.; Jagdale, S.; Potamialis, C.; Bowers, J. W.; Walls, J. M.; Munshi, A. H.; Barth, K. L.; Sampath, W. S. Degradation of Mg-doped Zinc Oxide Buffer Layers in Thin Film CdTe Solar Cells. *Thin Solid Films* **2019**, *691*, 137556.
(28) Togay, M.; Greenhalgh, R.; Shimpi, T.; Walajabad, S. S.; Barth, K. L.; Walls, J. M.; Bowers, J. W. In Transient Metastable Behaviour in Highly Efficient MZO/CdSeTe/CdTe Thin Film Solar Cells. *2021 IEEE 48th Photovoltaic Specialists Conference (PVSC)* **2021**, *2021*, 0637−0642.
(29) Kephart, J. M.; McCamy, J. W.; Ma, Z.; Ganjoo, A.; Alamgir, F. M.; Sampath, W. S. Band Alignment of Front Contact Layers for High-Efficiency CdTe Solar Cells. *Sol. Energy Mater. Sol. Cells* **2016**, *157*, 266−275.
(30) Ablekim, T.; Duenow, J. N.; Zheng, X.; Moutinho, H.; Moseley, J.; Perkins, C. L.; Johnston, S. W.; O'Keefe, P.; Colegrove, E.; Albin, D. S.; et al. Thin-Film Solar Cells with 19% Efficiency by Thermal Evaporation of CdSe and CdTe. *ACS Energy Letters* **2020**, *5* (3), 892−896.

https://doi.org/10.1021/acsaem.2c00153
ACS Appl. Energy Mater. XXXX, XXX, XXX−XXX